Chemistry–A European Journal
Research Article
doi.org/10.1002/chem.202402094
Chemistry Europe
European Chemical Societies Publishing
www.chemeurj.org

Neutral and Anion Species of Quinoidal Thienothiophene Diketopyrrolopyrroles Display a Common Aggregation Mode

Sergio Moles Quintero[+],[a] Maria João Álvaro-Martins[+],[b] Daniel Aranda,*[c] Yonghao Zheng,[d] Juan Aragó,[c] Enrique Ortí,[c] Ángela Sastre Santos,*[b] and Juan Casado*[a]

A comprehensive investigation of two new molecular triads incorporating the diketopyrrolopyrrole unit into a quinoidized thienothiophene skeleton, which is further end-capped with dicyanomethylene (**DPP-TT-CN**) or phenoxyl groups (**DPP-TT-PhO**), has been carried out. A combination of UV-Vis-NIR and infrared spectroelectrochemical techniques and cryogenic UV-Vis-NIR absorption spectroscopy supported by theoretical calculations has been used. The main result is the formation of similar H-aggregates in the dimerization process of the neutral molecules and of the charged anionic species. The experimental absorption spectra of the aggregated species are accurately reproduced by quantum chemical calculations using the Spano's model, including excitonic coupling for the dimeric forms and full vibronic resolution of the absorption bands. The strong excitonic coupling taking place is key to understand the electronic structure of the dimeric and has been instrumental to disentangle the type of H-aggregation. This study is of relevance to get a better understanding of the molecular aggregation of organic π-conjugated chromophores and is useful as a guideline for the refinement of the engineering of molecular materials for which supramolecular design is required.

Introduction

Originally, charged π-conjugated oligomers were largely investigated as models of the structural and electronic impact that doping has in π-conjugated conducting polymers.[1] More recently, the interest of "molecular" doping point towards optimizing processes in, for instance, thermo-power devices for energy conversion, charge accumulation in batteries, etc.[2] By themselves, π-conjugated molecules in neutral state were first implemented as organic molecular semiconducting substrates in organic field-effect transistors (OFETs). This triggered out great efforts to improve their solid-state or supramolecular disposition pursuing maximal intermolecular overlap for enhanced charge transport.[3] In any case, the understanding of how neutral or charged molecules interact to form aggregates or more complex supramolecular organizations is of prime relevance.[4]

π-Conjugated compounds have been demonstrated to display unique properties of aggregation due to the existence of planar π-surfaces which drive different forms of π–π-stacking.[5] According to the simple Kasha model of aggregation in basic molecular dimers, two main modes were described.[6] On one hand, H-type aggregation (i.e., head-to-head intermolecular coupling), which is revealed by an hypsochromic shift (i.e., blue shift) of the main or strongest absorption band. On the other hand, J-type aggregation (i.e., head-to-tail intermolecular coupling), that produces a bathochromic or red shift of the strongest absorption band from the monomer to the dimer.[7] However, when vibronic resolution is available, the aggregate-type assignment based on Kasha model can be misleading and other effects besides excitonic coupling must be taken into account. In these situations, more complete models like those proposed by Spano[8] must be utilized. Both H- and J-type aggregations have been thoroughly discussed in the literature including systems that are able to transit from one aggregation pattern to the other, and even with few cases in which H–J aggregation or mixed H- and J-aggregation coexist.[10]

Quinoidal oligothiophenes mainly constructed by dicyanomethylene encapsulation and incorporating 3/4 thiophene rings have been extensively used in organic electronic as semiconducting substrates for *n*-channel OFETs (Figure 1).[11,12,13,14] The relevance of π–π-stacking in the electrical output of the OFET devices has been well recognized and analysed in detail

[a] S. Moles Quintero,[+] J. Casado
Department of Physical Chemistry, Faculty of Science, University of Málaga, 29071 Málaga, Spain
E-mail: casado@uma.es
[b] M. João Álvaro-Martins,[+] Á. Sastre Santos
Área de Química Orgánica, Instituto de Bioingeniería, Universidad Miguel Hernández, 03202 Elche, Spain
E-mail: asastre@umh.es
[c] D. Aranda, J. Aragó, E. Ortí
Instituto de Ciencia Molecular (ICMol), Universidad de Valencia, 46980 Paterna, Spain
E-mail: daniel.aranda@uv.es
[d] Y. Zheng
School of Optoelectronic Science and Engineering, University of Electronic Science and Technology of China (UESTC), 610054 Chengdu, P. R. China
[+] S. M. Q. and M.J.A.-M. contributed equally to this work.
Supporting information for this article is available on the WWW under https://doi.org/10.1002/chem.202402094

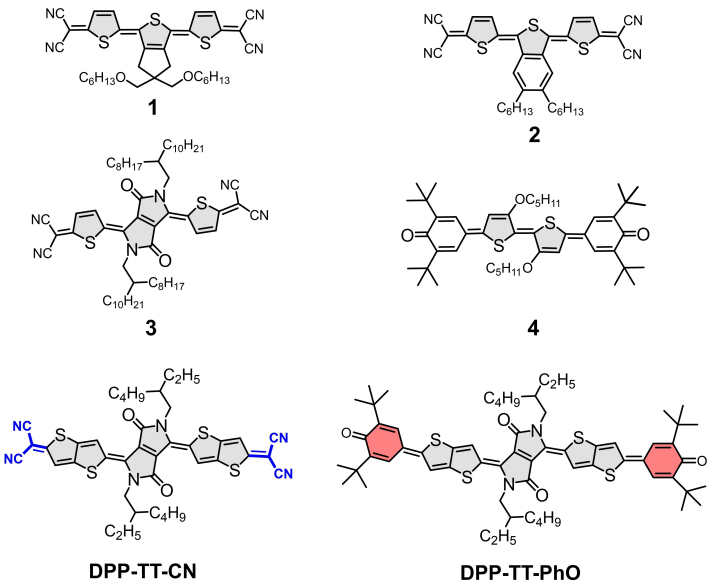

Figure 1. a) Quinoidal oligothiophenes bearing bis(diciyanomethylene) and bis(benzosemiquinone) endcapping groups (**1**–**4**). b) Quinoidal **DPP-TT-CN** and **DPP-TT-PhO** compounds studied in this work.

in the work of Miller, Brédas and coworkers.[15,16] However, despite the numerous quinoidal molecules prepared and the crystalline structures reported, the phenomenon of aggregation in solution, as the potential seed for further solid-state organization, has not been addressed in detail. Indeed, for the known thienoquinoidal oligomers, their optical properties in thin solid films and as a function of the annealing temperatures have been studied only for a few compounds (**1**–**4** in Figure 1).[17,18,19,20] Yet, for any of these, further analysis discussing the type of aggregation in the context of their optical and electronic properties in solution in their neutral states has not been performed.

Complementarily to the Kasha's pioneering studies on the consequences of dimerization/aggregation in the optical properties of neutral π-conjugated molecules, the aggregated states of *charged species* gained interest in the molecular electronics field to understand charge transport in organic materials. Seminal works on the dimerization, for instance, of aromatic π-conjugated oligothiophene radical cations in solution were first described by Larry L. Miller in the late 80's of the last century.[21,22,23] Whereas aromatic oligothiophenes have been shown to form different classes of molecular aggregates in the neutral state, studies in which the mode of aggregation in the neutral state is demonstrated to be also efficient in the charged state are scarce or inexistent. It turns out that the attainment of molecules that can form aggregates both in charged and neutral states in solution is certainly welcome to enrich the understanding of their aggregation and to improve our precision in the design of molecular building blocks for charge transport, energy conversion and storage, etc.

The combination of diketopyrrolopyrroles (DPPs) and oligothiophenes, the latter in the form of thienoquinoidal skeletons such as those shown in Figure 1, have provided interesting systems ranging from closed-shell structures to diradical open-shell species.[24,25,26] The mixing of quinoidal oligothiophenes with DPP cores in order to broaden the capability of these molecules as functional materials has been already reported and implemented in several successful applications.[27,28] In addition, DPPs with phenoxyl encapsulation and quinoidal branches by benzene, thiophene, furane or selenophene have been reported and the electronic properties of the neutral and of the reduced anionic species interpreted in terms of intramolecular parameters such as the aromaticity of the bridging units, their mixed valence properties, among others.[24]

In this article we have synthetized two new DPP based compounds, both disubstituted with quinoidal thienothiophene units (TT), which are terminally endcapped with dicyanomethylene groups (CN) or phenoxyl groups (PhO), that is, the molecular triads hereafter referred as **DPP-TT-CN** and **DPP-TT-PhO**, respectively (Figure 1b). With these molecules in hands, we will afford the discussion of the electronic and structural properties of their molecular aggregates in solution either in the neutral state as in the charged anionic forms. There are not many cases in which persistent and substantial *aggregation in solution* of *neutral and charged species of the same molecule* can be realized. For this end, a set of spectroscopic studies based on electronic UV-Vis-NIR absorption spectra recorded as a function of temperature and UV-Vis-NIR and infrared spectroelectrochemical experiments are carried out in combination with theoretical molecular modelling using the exciton model of Spano suited for the interpretation of the optical properties of aggregates.

Results and Discussion

Synthesis

DPP-TT-PhO was synthesized by a Suzuki-Miyaura cross-coupling between the respective dibromo **DPP-1** and the boronic ester to obtain **DPP-2** in 68% yield, followed by oxidation with PbO_2 in 95% yield (Scheme 1). **DPP-TT-CN** was newly synthesized from dibromo **DPP-1** in the presence of sodium malononitrile through Pd-catalysed Takahashi coupling reaction followed by aerial oxidation with 46% yield (Scheme 1). With this protocol, brominated side products described when saturated brominated water was used, were fully avoided.

The synthesis of **DPP-1** and the respective oxidation were previously described in the literature.[29] **DPP-TT-PhO** presented good solubility in common organic solvents, including $CHCl_3$, CH_2Cl_2, and toluene. In contrast **DPP-TT-CN** demonstrates only partial solubility in $CHCl_3$ and ethyl acetate, but exhibits satisfactory solubility in CH_2Cl_2. The lower solubility of **DPP-TT-CN** is attributed to its more rigid backbone that extends all over the conjugated skeleton between the endcapping dicyanomethylene units.[25] The chemical structures of **DPP-2** and **DPP-TT-CN** derivatives were elucidated using ^1H and ^{13}C NMR, FT-IR, and MALDI-TOF mass spectrometry techniques (Figure S1–S4 and S5–S8). For **DPP-TT-CN** we use CD_2Cl_2 with a drop of THF-d to eliminate the π-π staking to get a well-defined ^1H and ^{13}C NMR spectra. However, for **DPP-TT-PhO**, characterization was performed by FT-IR (Figure S9) and HR-MALDI-TOF MS in negative mode (Figure S10), due to silent NMR after PbO_2 oxidation because of their paramagnetic behaviour.

Electronic Properties and Aggregation Behaviour of the Neutral Species

UV-Vis Spectra at 300 K and the Molecularly Dissolved Species

Figure 2 shows the electronic absorption spectra of **DPP-TT-CN** and **DPP-TT-PhO** at room temperature in CH_2Cl_2 solution. The 300 K spectra of both compounds display the typical features of thienoquinoidal derivatives. For instance, a strong low-energy absorption at 765 nm in **DPP-TT-CN** accompanied by a weaker band at shorter wavelengths, at 695 nm, which corresponds to a spacing of about 1300 cm^{-1} revealing the vibronic origin of the two bands. For **DPP-TT-PhO**, this pair of bands is recorded at 879 nm, the strongest band, and at 795 nm, the weaker satellite, accounting for a vibrational progression of approximately 1250 cm^{-1}. The overall redshift from 765 to 879 nm on replacing the cyano by the phenoxyl groups is the result of extending the conjugated structure with two additional phenoxyl groups.

Quantum chemical calculations of the electronic spectra of **DPP-TT-CN** and **DPP-TT-PhO** were carried out by first consider-

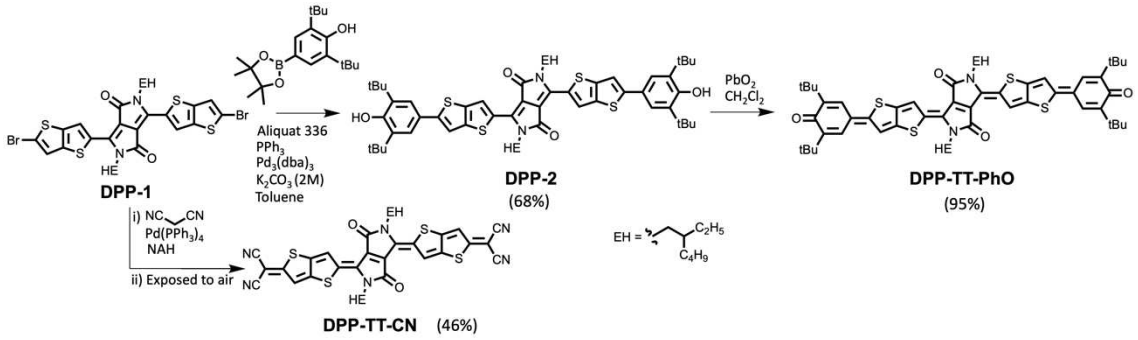

Scheme 1. Synthesis of DPP-TT-CN and DPP-TT-PhO.

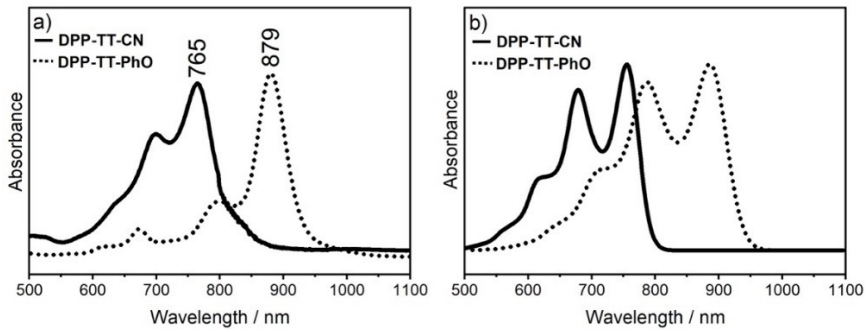

Figure 2. a) UV-Vis-NIR absorption spectra of the two studied compounds in approximately 10^{-5} M concentration at 300 K in CH_2Cl_2. b) Theoretical spectra calculated at the CAM-B3LYP/6–31 G(d,p) level of theory (closed-singlet configuration) including the vibronic structure using the FC|VG approach. The calculated spectra were shifted by −0.295 and −0.140 eV for **DPP-TT-CN** and **DPP-TT-PhO**, respectively, to superpose the lowest energy band with experiments. Stick transitions were convoluted with gaussian functions of half width at half maximum (HWHM) of 0.04 eV.

ing the vertical excitations resulting from TD-DFT calculations, which predict the lowest-energy $S_0 \rightarrow S_1$ transition at 588 nm for **DPP-TT-CN** and at 724 nm for **DPP-TT-PhO** (see the Supporting Information for full computational details). When vibronic resolution is added, the lowest energy bands are located at 642 and 806 nm to be correlated with the experimental bands at 757 and 879 nm, respectively. TD-DFT calculations reproduce the red shift in going from **DPP-TT-CN** to **DPP-TT-PhO** but overestimate the energy of the absorption bands. This is typical and expected when using the CAM-B3LYP functional. On these vertical excitations, their vibronic structures were computed using the Vertical Gradient (VG) model and the Franck-Condon approximation (FC).[30,31] The vibronic progressions arise from two different CC stretching vibrational modes with wavenumbers around 1550–1590 and at 1043 cm^{-1} (Figure S11), whose convolution results in a single spectral band. The former vibrational mode delineates a quinoid-to-aromatic transformation involving also the $C(CN)_2$ or PhO groups, which explains the different wavenumber obtained for each molecule, whereas the latter is more localized on the DPP unit and therefore has an almost identical value for both systems. The theoretical simulation of the vibronic structure reveals a nice fitting between theory and experiment for the electronic spectra of **DPP-TT-CN** and **DPP-TT-PhO** (Figure 2). It predicts correctly the position of the vibronic progressions and also the relative intensities for **DPP-TT-CN**. For **DPP-TT-PhO**, the progression is however overestimated probably by the difficulties of standard theoretical methods to simulate the properties of systems with low-lying quinoid/aromatic transformations.

UV-Vis Spectra at 80 K and the Formation of Aggregated Species

Figure 3 displays the absorption spectra of the two compounds in solution of methyl tetrahydrofuran (methyl-THF) as a function of temperature. The methyl-THF solution of **DPP-TT-PhO** shows two distinctive effects upon cooling: i) a small red-shift of the absorption spectrum as a whole by 10–20 nm (about 200 cm^{-1} in this region) without any further change in the overall shape of the vibronic peaks when going from room temperature to 140 K (Figure 3c); and ii) an interexchange of intensity between the 0–0 and 0–1 vibronic bands in the temperature interval from 140 to 80 K (Figure 3d), in which the 0–1 band (817 nm at 140 K and 860 nm at 80 K) becomes the most intense in detriment of the 0–0 band (897 nm at 140 K and 909 nm at 80 K). A new weak band corresponding to the 0–2 transition appears at 817 nm as a consequence of the stronger vibronic progression observed in this temperature range and the modification of the spacing between bands from 1092 cm^{-1} at 140 K to 627 cm^{-1} at 80 K. For **DPP-TT-CN** a similar behaviour is found on cooling (Figure 3a, b), the main differences with respect to **DPP-TT-PhO** being: i) the intensity exchange of the strongest band starts at 160 K; and ii) the spacing is larger, 1238 cm^{-1} between the longest wavelength band at 775 nm and the shortest wavelength band at 703 nm.

The changes at low temperature of the main electronic absorption band of **DPP-TT-CN** and **DPP-TT-PhO** can be interpreted as a consequence of the formation of H-type dimer, which typically display hypsochromic displacements of the strongest bands towards shorter wavelengths. Accounting for vibrational resolution, **DPP-TT-CN** and **DPP-TT-PhO** maxima are respectively shifted from 770 and 897 nm (0–0 vibronic bands) to 703 and 860 nm (0–1 vibronic bands), in agreement with

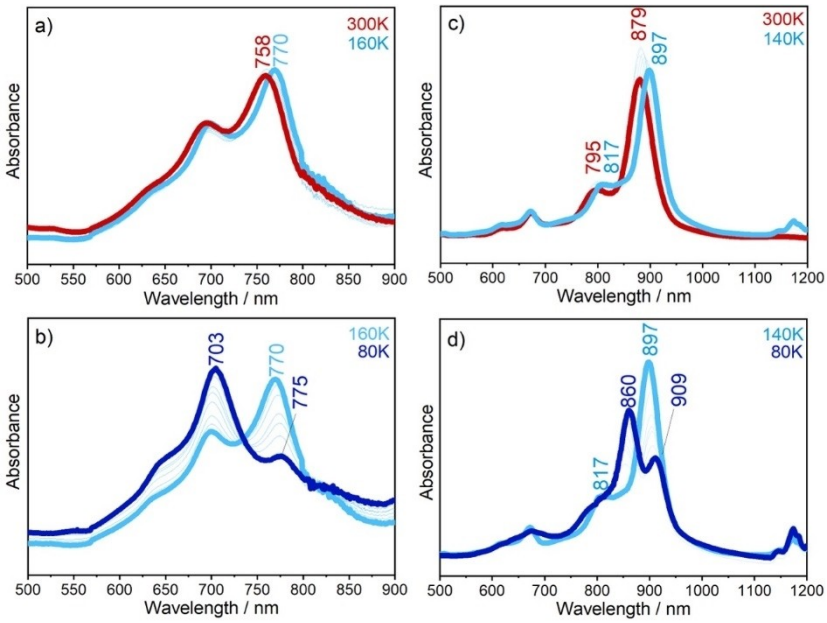

Figure 3. UV-Vis-NIR absorption spectra as a function of temperature of 10^{-5} M solutions in 2-methyl THF. Left: **DPP-TT-CN** in the 300–160 (a) and 160–80 K (b) intervals. Right: **DPP-TT-PhO** in the 300–140 (c) and 140–80 K (d) intervals.

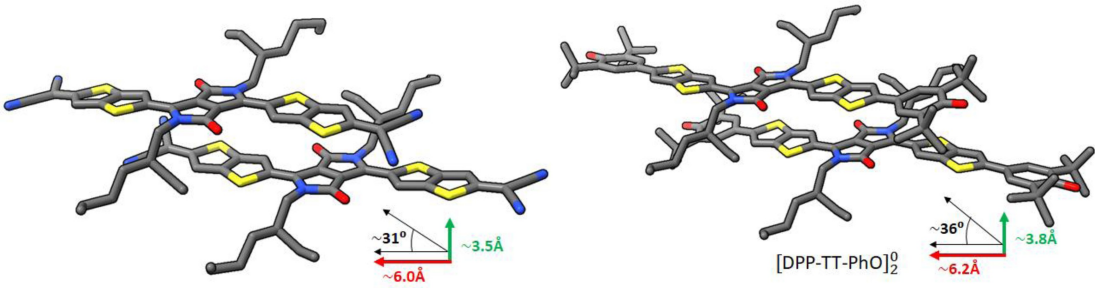

Figure 4. CAM-B3LYP/6–31 G(d,p)/GD3-optimized dimer structures calculated for **DPP-TT-CN** (left) and **DPP-TT-PhO** (right). The stacking (in green) and sliding distances (in red) are shown for each compound together with the angle formed by the line joining the center of mass of both monomers and the long molecular axis (in black). Figure composed with ChimeraX 1.5.

what is expected from Kasha's rule applicable when no vibronic resolution is available. An additional argument for the occurrence of H-type aggregates in low temperature solutions concerns the relative intensity of the two peaks of the spectrum of **DPP-TT-PhO** at 80 K (860 and 909 nm spaced by 627 cm^{-1}). Spano has shown that Kasha's theory for aggregates must be completed by accounting for vibrations when strong excitonic couplings take place.[7—10] This is seemingly the case for **DPP-TT-CN** and **DPP-TT-PhO**, which gives rise to remarkable changes in the vibronic peaks of the absorption spectra.

Unfortunately, no crystal could be obtained for the quinoidal compounds under study, from which the experimental molecular structure and the supramolecular organization could not be analysed. However, there is abundant literature for the solid-state structure of aromatic thiophene-DPP derivatives and, in particular, the molecular structure and crystal ordering of a similar DPP compound with a simpler thiophene unit and a phenyl ring (**DPP-T-Ph**, see Figure S13) with identical alkyl chains was resolved.[32] This structure consists of stacked monomers, which are significantly displaced along the long molecular axis to accommodate the voluminous alkyl chains attached to the DPP core. The structure of the dimers observed in the crystal structure reported for **DPP-T-Ph** were taken as a structural model for the dimerization of our compounds. Thus, dimers of **DPP-TT-CN** and **DPP-TT-PhO** were constructed simply by replacing the **DPP-T-Ph** units by the **DPP-TT-CN** and **DPP-TT-PhO** monomers as shown in Figure 4. The geometries of the resulting dimers were fully relaxed at the DFT level. For **DPP-TT-CN**, the optimized dimer shows a π-stacking distance of ~3.5 Å, a sliding distance of about 6.0 Å and an angle between the line joining the center of mass of the monomers and the long molecular axis of 31^0 (Figure 4). Noteworthy, for **DPP-TT-PhO** the additional steric hindrance derived from the tert-Bu groups increases both distances and the angle to 3.8 Å, 6.2 Å and 36^0 respectively.

The parameters of the excitonic Hamiltonian used for the theoretical simulation of the spectra of the aggregated species are collected in Table 1. The monomer excitation energy E_i, the gas-to-crystal energy shift Δ and the Huang-Rhys factor for an effective mode responsible of the progression λ_{HR} were empirically adjusted to fit the position and shape of the peaks in the experimental spectra (Figure 5a,c), whereas the frequency of the effective mode ω_{eff} and the excitonic coupling constant J_{ij} were derived from calculations as described in the electronic supplementary material. Although J_{ij} was computed for a dimer, the spectra from the excitonic Hamiltonian were obtained for a decamer (N = 10) assuming that all interacting monomers have the same J_{ij}. It has been confirmed that the spectrum is converged with N = 10, i.e., it does not change by increasing the size of the aggregate. The aim is to obtain the parameters that reproduce the experimental spectra of the monomers and combine these parameters with the J_{ij} calculated for the proposed molecular arrangement. Then, if the spectrum recorded experimentally for the aggregate is reproduced with the excitonic Hamiltonian, the arrangement used to calculate J_{ij} is expected to be plausible. Therefore, the monomer spectra shown in Figure 5b,d are not fully identical to the theoretical spectra shown in Figure 2b, which were fully obtained from *ab initio* calculations. The theoretical spectra obtained for the aggregates by the application of Spano's excitonic coupling model have to be compared with the experimental spectra recorded at 80 K in Figure 5a,c. For both molecules, an increase of intensity is predicted for the band associated to the 0–1 transition of the experimental peaks at 703 and 860 nm for **DPP-TT-CN** and **DPP-TT-PhO**, respectively, at the cost of the 0–0 band (770 and 897 nm for **DPP-TT-CN** and **DPP-TT-PhO**, respectively), which shows the highest intensity at higher temperatures. This trend is a characteristic feature of H-aggregates and fully agrees with the behavior observed experimentally, thus supporting the formation of H-type aggregated species upon cooling. The structures proposed in

Table 1. Parameters of the Frenkel excitonic Hamiltonian. J_{ij}^{corr} was used to calculate the spectra.

	DPP-TT-CN	DPP-TT-PhO
E_i (eV)	1.51	1.36
Δ (eV)	0.06	0.12
ω_{eff} (cm^{-1})	1300	1300
λ_{HR}	0.60	0.15
J_{ij}^{gas} (eV)	0.135	0.136
J_{ij}^{sol} (eV)	0.085	0.083
J_{ij}^{corr} (eV)	0.070	0.069

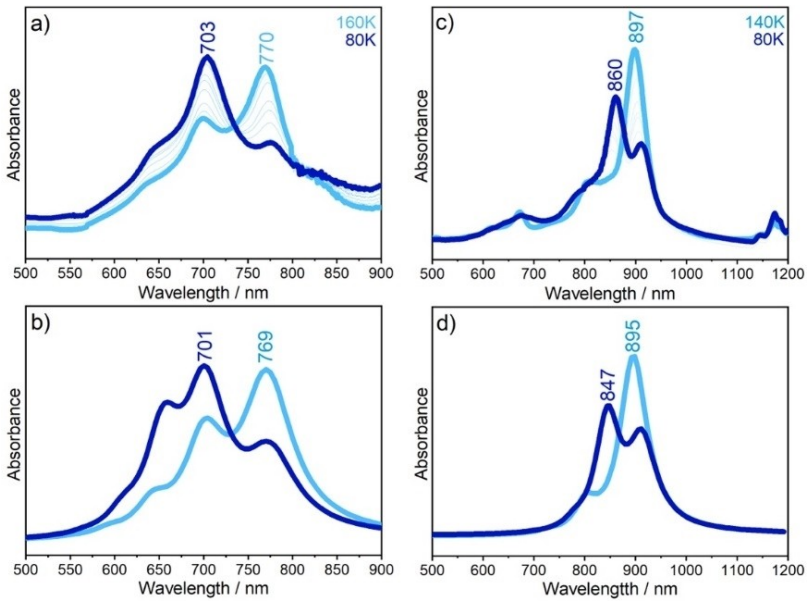

Figure 5. Comparison of experimental (top) and calculated (bottom) spectra for **DPP-TT-CN** (a and b) and **DPP-TT-PhO** (c and d). In the (a) and (c) panels, the sky blue color corresponds to the 160 and 140 K UV-Vis spectra while the deep blue color refers to the spectra at 80 K. In the b and d panels, the sky blue color corresponds to the spectra calculated for the monomers and the deep blue color belongs to the aggregates. Calculated spectra obtained from the diagonalization of the Frenkel excitonic Hamiltonian. Calculated transitions were convoluted with Gaussian functions of HWHM = 0.06 and 0.025 eV for **DPP-TT-CN** and **DPP-TT-PhO**, respectively.

Figure 4 for **DPP-TT-CN** and **DPP-TT-PhO**, based on the crystal structure reported for the closely related **DPP-T-Ph** molecule, reproduce the spectra recorded at low temperature and therefore constitute a robust proposal for the aggregate structure obtained upon cooling.

The visualization of the monomer-to-dimer reaction in solution at such low temperatures has been rarely reported and certainly unprecedented. This can be explained by the weakness of the Coulombic dipole-dipole forces, which are cancelled by thermal fluctuation and entropy forces. In fact, we were unable to find such low-temperature transformation in the parent compound with thiophene (T) instead of TT units (**DPP-T-PhO**) (see the UV-Vis spectra recorded in methyl-THF as a function of the temperature, from 300 K to 80 K, for the shorter **DPP-T-PhO** whose chemical structure is displayed in Figure S13). A plausible explanation for the absence of the low-temperature transformation associated to aggregation is the smaller π-surface for intermolecular interactions exhibited by **DPP-T-PhO**, which results insufficient to circumvent the solution entropy forces in the range of temperatures down to 80 K. By increasing the available π-surface, together with the increased rigidity of the thienothiophene moiety in **DPP-TT-CN** and **DPP-TT-PhO**, the aggregation enthalpy increases in absolute value thus elevating the temperature at which dimerization/aggregation takes place above 80 K.

Electronic Properties and Aggregation Behaviour of the Charged Anionic Species

Electrochemical Properties

The electrochemical properties were explored through cyclic voltammetry using CH_2Cl_2 as solvent containing 0.1 M tetrabutylammonium hexafluorophosphate ($TBAPF_6$) as supporting electrolyte (Table 2 and Figure S14). A notable observation from the comparison between the cyclic voltammetry of **DPP-TT-PhO** and its precursor (**DPP-2**) is the distinct first reduction potential exhibited by the **DPP-TT-PhO** derivative at −0.65 eV. In the case of **DPP-TT-CN**, owing to its marked electron-acceptor character, two reduction waves at low potentials (−0.40 and −0.60 V) are observed and no oxidation is recorded during anodic sweeping. The two-electron reduction process involves the conversion of the π-system into a radical anion, succeeded by the formation of the dianion stabilized by the electron-withdrawing terminal dicyanomethylene groups.

Table 2. Optical and electrochemical parameters of **DDP-2**, **DPP-TT-PhO** and **DPP-TT-CN**.

Compound	$E_{g,CV}$ (eV)[a]	LUMO/HOMO (eV)[b]
DPP-2	1.83	−3.19/−5.02
DPP-TT-PhO	0.89	−4.15/−5.04
DPP-TT-CN	–	4.40/–

– No value. [a] $E_{g,CV} = E_{LUMO} - E_{HOMO}$. [b] $LUMO = -4.8 - E^{Red1}_{1/2}$. $HOMO = -4.8 - E^{Ox1}_{1/2}$.

UV-Vis-NIR Absorption Spectroelectrochemistry

UV-Vis-NIR spectroelectrochemical studies were carried out for **DPP-TT-CN** and **DPP-TT-PhO** and are shown in Figure 6. Reduction of **DPP-TT-CN** up to its first reduction wave of the cyclic voltammetry produces a spectrum with medium-intensity and weak bands at 1006 and 1629 nm, respectively, which are typical bands of radical anions of quinoidal oligothiophenes generally reported at 1007 and 1642 nm.[33,34,35,36] The similitude of the spectra of the radical anion of these quinoidal oligothiophenes and of **DPP-TT-CN** reveals the main role of the charge delocalization between the two thienothiophene arms featuring a mixed-valence structure in which two acceptors compete for the added charge.[24] An interesting aspect is that the electron acceptor DPP unit acts apparently as mediator of the charge delocalization without further electron-withdrawing effect possibly because of the cross-conjugated structure of the DPP unit regarding the inter-dicyano long π-conjugated path.[36,37] In addition to this pair of absorption bands, there is another intense absorption feature at 816 nm which grows up in parallel with the 1006/1629 nm pair of bands upon reduction.

Reduction of **DPP-TT-CN** was also carried out by chemical titration with cobaltocene starting with a more diluted 10^{-5} M solution (Figure 6d, i.e., compared with the 10^{-3} M solution used in the spectroelectrochemical experiment in Figure 6a), from which the same first reduced species is obtained with the same three 816/1006/1629 nm bands but differing in the absorbance ratios, the 816 nm band being weaker than the other two (compare Figures 6c – top – and 6d). This invokes the hypothesis that there is a concentration dependent aggregation process of the radical anion formed upon reduction, with the 816 nm band due to the aggregated species (i.e., grows up with increasing concentration). In oligothiophenes, π-dimers of radical cations and anions, or dicationic and dianionic dimers, are characterized by a blue-shift of the absorption bands compared to the singly charged monomer.[21–23] This is a consequence of the bonding interaction between the two radicals in dications and dianions, which are able to overcome the electrostatic repulsion generated by dimerization/aggregation. To further check this, the same dilute 10^{-4} M solution was cooled down in a controlled manner to 180 K and found that there is an increase of the absorbance of the 816 nm band on lowering the temperature at the expenses of the molecularly dissolved radical anion bands at 1006/1629 nm (Figure 6c, bottom). In addition, another band appears at 1208 nm at low temperatures, which is presumably linked with the 816 nm feature, but much weaker, and that is only observed when the aggregated species is largely predominant. These two bands at 816 and 1208 nm are thus characteristics of the anionic aggregate or diradical dianion π-dimer of **DPP-TT-CN** ([**DPP-TT-CN**]$_2^{2-}$). Dimerization or larger aggregation of radical cations of π-conjugated molecules is a well-known and largely documented phenomenon; however, the same processes in negatively charged π-systems are much less known, and a rather limited number of cases has been reported.[36–39]

Additional electrochemical reduction of the first generated π-dimer dianion/anionic aggregate gives rise to the full disappearance of its bands followed by the formation of a new absorption feature at 754 nm owing to the formation of a dianion species of an individual **DPP-TT-CN** ([**DPP-TT-CN**]$^{2-}$) (Figure 6a). Dianions of quinoidal oligothiophenes typically give rise to UV-Vis-NIR absorption spectra with dominant bands placed in the 500–600 nm spectral region close to that typically

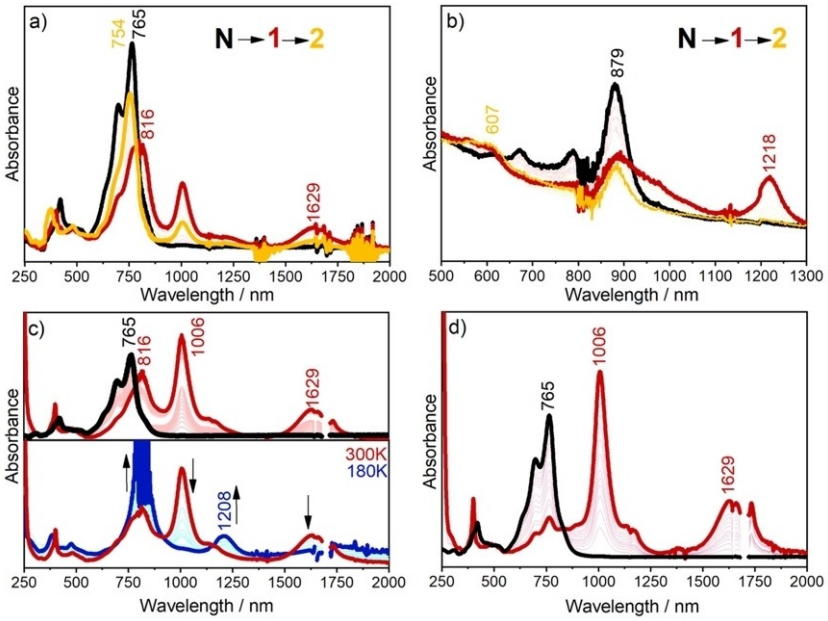

Figure 6. UV-Vis-NIR spectroelectrochemical reduction in the 0–1.5 V interval of **DPP-TT-CN** (a) and **DPP-TT-PhO** (b) recorded at a 10^{-3} M concentration in CH_2Cl_2, 0.1 M $TBAPF_6$ at 300 K. c) Chemical titration of **DPP-TT-CN** 10^{-4} M with cobaltocene at 300 K (top) and by lowering the temperature to 180 K (bottom). d) Chemical titration of **DPP-TT-CN** 10^{-5} M with cobaltocene at 300 K.

found for neutral aromatic oligothiophenes.[33–35] In this case, however, the band of the dianion/anionic aggregate is detected at longer wavelengths owing to the particular role of the DPP unit, which acts draining negative charge from the TT units in a sort of push-pull effect that displaces the absorption to the red part of the spectrum in comparison with the bands recorded for dianions of quinoidal oligothiophenes without this central electron accepting unit.[35]

To further explore the formation of molecular aggregates upon reduction, the vibrationally-resolved theoretical spectra were calculated for the radical anion ([**DPP-TT-CN**]$^{-\bullet}$) and dianion ([**DPP-TT-CN**]$^{2-}$) species of **DPP-TT-CN**. In addition, to simulate the charged aggregate, a dimeric species formed by two radical anions, [**DPP-TT-CN**]$_2^{2-}$, was considered. This dimer was obtained starting from the structure calculated for the neutral parent dimer and optimized upon appropriate inclusion of two negative charges forming a singlet ground electronic state dianion species. The supramolecular structure of the diradical dianion π-dimer resulted to be very similar to that calculated for the neutral dimer, with stacking and sliding distances of 3.5 and 6.2 Å, respectively, and an intermolecular angle between the line connecting the centers of mass of both monomers and the long molecular axis of 30°.

The vibronically resolved spectra calculated for the reduced species of **DPP-TT-CN** are represented in Figure 7 and the vertical excitation energies and main vibronic bands are summarized in Table 3. Two bright states are predicted for the radical anion [**DPP-TT-CN**]$^{-\bullet}$. The first is associated to the $D_0 \rightarrow D_1$ transition and provides a strong vibronic progression with two peaks at 2188 and 1675 nm, of which the first falls out of the spectral range of interest while the second matches nicely with the experimental band at 1629 nm. The second bright state, corresponding to the $D_0 \rightarrow D_3$ photoexcitation, shows a weaker progression whose maximum is located at 1027 nm and fits nicely with the 1006 nm experimental bands. Most importantly, no counterparts for the 816 (strong) and 1230 nm (weak) experimental bands were found for the [**DPP-TT-CN**]$^{-\bullet}$ species.

The electronic spectrum computed for the dimer dianion species [**DPP-TT-CN**]$_2^{2-}$ also shows two bright states associated to the $S_0 \rightarrow S_2$ and $S_0 \rightarrow S_5$ transitions (Table 3 and Figure 7). Both are characterized by very weak progressions basically consisting of a single peak, resulting in two new bands at 1209 nm ($S_0 \rightarrow S_2$) and 775 nm ($S_0 \rightarrow S_5$) that can be assigned to the 1230 and 816 nm experimental features. This is in total correspondence with the experiments at low temperature (Figure 6c, bottom), where the two bands associated to the dimer species (1230 and 816 nm) are the only ones observed while the bands ascribed to the monomer (1629 and 1006 nm) fully disappear. Therefore, the spectra observed for the reduced species is fully explained

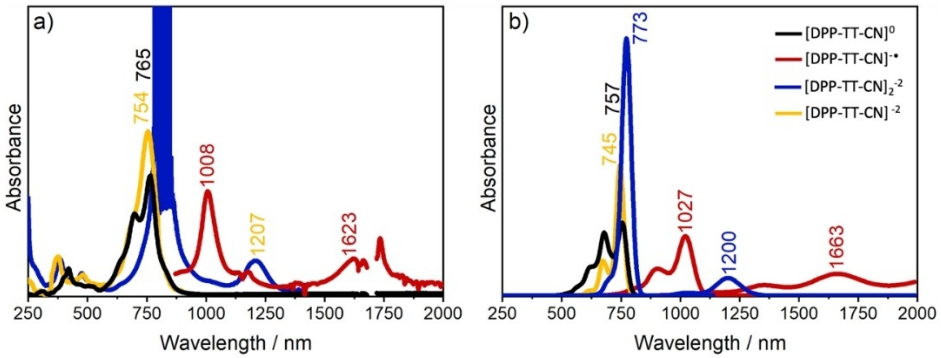

Figure 7. Experimental (a) and calculated FCVG (b) spectra for neutral [**DPP-TT-CN**] and its reduced species [**DPP-TT-CN**]$^{-\bullet}$, [**DPP-TT-CN**]$_2^{2-}$ and [**DPP-TT-CN**]$^{2-}$. The calculated spectra were shifted by −0.295 eV and all stick transitions were convoluted with gaussian functions of HWHM = 0.04 eV. Theoretical spectra calculated at the CAM-B3LYP/6–31 G(d,p) level of theory for the monomeric species and CAM-B3LYP/6–31 G(d,p)/GD3 for the dimer.

Table 3. Vertical excitation energies (*E*) and electric transition dipole moment dipole strengths ($|\boldsymbol{\mu}_{if}|^2$) calculated at the CAM-B3LYP/6–31 G(d,p) level of theory for the main excited states of the **DPP-TT-CN** monomer in neutral, anion and dianion states and for the [**DPP-TT-CN**]$_2^{2-}$ dimer. The values in parenthesis, only given for bright states, show the calculated energy after vibronic resolution after applying a redshift of 0.295 eV to match the neutral monomer lowest energy band with the position of the experimental band.

System	Transition	*E* (eV)	*E* (nm)	$\lvert\boldsymbol{\mu}_{if}\rvert^2$ (a.u.)
[**DPP-TT-CN**]	$S_0 \rightarrow S_1$	2.11 (1.82)	588 (757)	50.53
[**DPP-TT-CN**]$^{-\bullet}$	$D_0 \rightarrow D_1$	1.02 (0.73)	1213 (1675/2188)	31.69
	$D_0 \rightarrow D_3$	1.60 (1.31)	777 (1027)	30.77
[**DPP-TT-CN**]$_2^{2-}$	$S_0 \rightarrow S_2$	1.35 (1.06)	917 (1209)	7.47
	$S_0 \rightarrow S_3$	1.75 (1.46)	709 (–)	0.00
	$S_0 \rightarrow S_4$	1.90 (1.61)	651 (–)	1.45
	$S_0 \rightarrow S_5$	1.91 (1.62)	649 (775)	68.22
[**DPP-TT-CN**]$^{2-}$	$S_0 \rightarrow S_1$	2.01 (1.72)	617 (748)	38.51

by combining the results for the [**DPP-TT-CN**]$^{-\bullet}$ monomer and the diradical [**DPP-TT-CN**]$_2^{2-}$ dimer as a representative of the aggregated forms. It is also worth mentioning that the 816 nm band in the experiment is notably broader than the other bands in the same spectrum. Calculations predict two additional excited states for the [**DPP-TT-CN**]$_2^{2-}$ species that are nearly degenerate with the bright $S_0 \rightarrow S_5$ transition (Table 3). Therefore, it can be expected that these three states are actually vibronically coupled, and the intensity redistribution associated to this coupling can be the source of the additional broadening of this experimental band and the shoulder about 740 nm.[40]

The spectrum calculated for the further reduced species [**DPP-TT-CN**]$^{2-}$ shows a single bright transition ($S_0 \rightarrow S_2$, Table 3) characterized by a weak progression with the lowest energy band at 748 nm, very close to the calculated value of the neutral monomer (765 nm). This is in perfect agreement with the experimental spectrum obtained at very negative potentials in Figure 6a (yellow line), that is indeed very similar to that of the neutral monomer but slightly blue-shifted to 754 nm and with a weaker progression mostly manifested as a shoulder around 740 nm. The excellent agreement between the theoretically simulated spectra calculated for the different reduced species and those experimentally recorded thus confirms the nature of the negatively charged species generated upon reduction.

For **DPP-TT-PhO**, a similar behaviour is found though the reduction transformations either electrochemically or chemically are less clear. Spectroelectrochemical reduction of **DPP-TT-PhO** produces the initial appearance of two main bands at 879 and 1218 nm (Figure 6b), which are assigned to the anionic aggregate or π-dimer dianion ([**DPP-TT-PhO**]$_2^{2-}$) and radical anion ([**DPP-TT-PhO**]$^{-\bullet}$), respectively, in correlation with the bands observed for these species at 816 and 1006 nm, respectively, in the concentrated solution of **DPP-TT-CN**. Experiments by chemical reduction in dilute solutions were unsuccessful due to the overall low solubility and absorbance of the compound. Posterior reduction of the π-dimer dianion of **DPP-TT-PhO** gives way to the appearance of a band at 607 nm assigned to the generation of the molecularly dissolved [**DPP-TT-PhO**]$^{2-}$ dianion.

Infrared Absorption Spectroelectrochemistry

The infrared absorption spectra recorded upon reduction in in-situ spectroelectrochemical conditions are shown in Figure 8 for **DPP-TT-CN**. In cyano-substituted compounds, the vibrational infrared spectra as a function of the reduction state are very informative of the structural and electronic properties of anionic species since there is a direct relationship between the reduction level and the charge density over the C≡N moieties and, as a result, the wavenumber at which the stretching mode of the C≡N group, hereafter referred as ν(C≡N), appears.[33–37] The antibonding character of the C≡N bond in the LUMO makes that charge injection lengthens the C≡N distance (i.e., weakens the triple bond) upon reduction and consequently decreases ν(C≡N). Therefore, a kind of proportionality between the degree/extension of the reduction state and the decrease of the ν(C≡N) wavenumber exists.

Figure 8a shows the evolution of the infrared ν(C≡N) band upon spectroelectrochemical reduction at 300 K. The starting point is the infrared spectrum of neutral **DPP-TT-CN**, for which the ν(C≡N) wavenumber is measured at 2210 cm^{-1}. Despite the presence of four C≡N moieties, only one intense band emerge for the ν(C≡N) modes, which is due to the antisymmetric vibration of the four bonds and is particularly intensified in the vibrational infrared spectrum (Figure S12). Upon reduction, at the initial stages of the cathodic process, the neutral ν(C≡N) band displaces up to 2200 cm^{-1} in a peak maximum that has a shoulder at 2187 cm^{-1}. The wavenumber position close to 2190 cm^{-1} is typical of the ν(C≡N) band of radical anions of tetracyano-substituted quinoidal oligothiophenes.[33—37] Here, the upshift to 2200 cm^{-1} might result from the electron-withdrawing effect of the central DPP unit that partially decreases the negative charge over the C≡N groups. However, the spectroelectrochemical experiment is carried out at 10^{-3} M concentration where π-dimers formed by coupling of radical anions and neutral molecules (mixed valence aggregate or [**DPP-TT-CN**]$_2^{-\bullet}$ dimers) are possibly formed. Reduction over these dimers mixed valence species might produce a delocalization of the charge over the two molecules thus decreasing the charge density on the terminal C≡N groups originating the 2200 cm^{-1} band. Reduction of the molecularly dissolved species

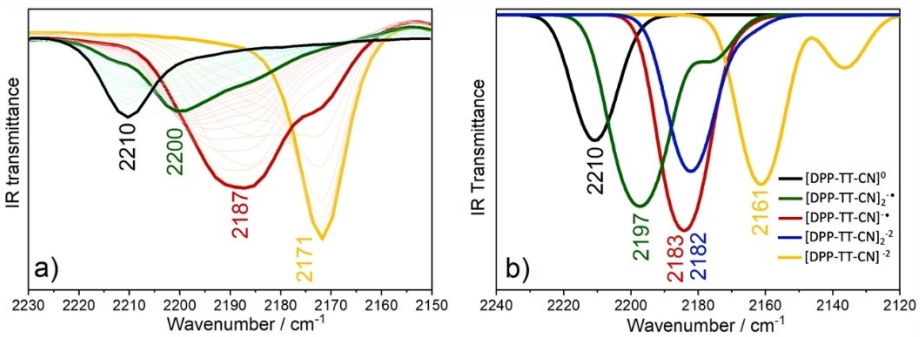

Figure 8. (a) Experimental fourier-transform infrared spectra recorded during electrochemical reduction in the 0 to −1.5 V interval of a 10^{-3} M solution of **DPP-TT-CN** in CH_2Cl_2, 0.1 M $TBAPF_6$ at 300 K. (b) Calculated IR spectra for the **DPP-TT-CN** species at the CAM-B3LYP/6–31 G(d) level of theory for monomeric specieis and CAM-B3LYP/6–31 G(d)/GD3 for dimers. Vibrational frequencies of all species were scaled by a factor of 0.9216 chosen to fit the calculated frequency of neutral **DPP-TT-CN** with the experimental value. All stick transitions were convoluted with gaussian functions of FWHM = 15 cm^{-1}.

produces the [**DPP-TT-CN**]$^{-\bullet}$ radical anion and the 2187 cm^{-1} band shoulder.

The 2187 cm^{-1} shoulder progress to be the main peak at higher reduction potentials becoming a broad ν(C≡N) band in the infrared spectrum extending from 2195 to 2185 cm^{-1} that additionally shows a shoulder at 2171 cm^{-1}. The wavenumber ν(C≡N) values typical of dianions of tetracyano-substituted quinoidal oligothiophenes are indeed found around 2170 cm^{-1}.[33–37] Therefore, whereas the 2171 cm^{-1} infrared band is assigned to the formation of the [**DPP-TT-CN**]$^{2-}$ dianion, the larger part of this band showing a continuous of transmittance in the 2195–2185 cm^{-1} interval can result from the formation of the anion dimeric species [**DPP-TT-CN**]$_2^{2-\bullet}$ or larger anionic aggregates. The large distribution of ν(C≡N) values might be also indicating the asymmetry of the formed dimers/aggregates such as evidenced by the quantum chemical modelling in which there is a displacement of one molecule relative to the other in the aggregate. This would make a distinctive environment for the dicyano-methylene groups, either those place in the internal part of the dimer and those in the outermost periphery, both bearing different amount of charge and thus different ν(C≡N) band values. The shoulder at 2171 cm^{-1} finally evolves to be the main peak of the infrared spectrum at higher reduction potentials due to the formation of the molecularly dissolved [**DPP-TT-CN**]$^{2-}$ dianion, which is formed upon dissociation of the dimers by electrostatic repulsion due to the accumulation of charge.

We have carried out quantum chemical calculations of the infrared spectra on the isolated molecules and in the aggregated forms which are shown in Figure 8b in comparison with the experimental values. In general, there is a very good agreement of the theoretical wavenumber values of the ν(C≡N) bands with those recorded experimentally. In particular, the calculations perfectly reproduce the progressive decrease on ν(C≡N) as more negative charge is added to the system by following the sequence **DPP-TT-CN**→[**DPP-TT-CN**]$^{-\bullet}$→[**DPP-TT-CN**]$^{2-}$ whose scaled wavenumbers for ν(C≡N) respectively are 2210, 2183 and 2161 cm^{-1} (see Figure S15 for displacement vectors). For dimers as representative of aggregates, the mixed value species [**DPP-TT-CN**]$_2^{-\bullet}$ displays a wavenumber value of 2200 cm^{-1} in between the neutral (**DPP-TT-CN**) and monoanion ([**DPP-TT-CN**]$^{-\bullet}$) monomers whereas the dimeric dianion [**DPP-TT-CN**]$_2^{-2}$ perfectly matches with the monomer with equivalent charge, [**DPP-TT-CN**]$^{-\bullet}$. These results support the conclusions already discussed above and suggest that the reference band at 2210 cm^{-1} indeed corresponds to the neutral monomer **DPP-TT-CN**, and the band after first reduction at 2200 cm^{-1} corresponds to the mixed valence [**DPP-TT-CN**]$_2^{-\bullet}$. Further reduction detected at 2187 cm^{-1} would result in species with one negative charge per monomer, either as the molecularly dissolved species [**DPP-TT-CN**]$^{-\bullet}$ or as aggregate with [**DPP-TT-CN**]$_2^{2-}$ as representative case. Finally, the most reduced species obtained experimentally at 2171 cm^{-1} can be assigned to [**DPP-TT-CN**]$_2^{-2-}$.

Among the species detected in the infrared spectroelectrochemical experiment, that corresponding to the mixed-valence [**DPP-TT-CN**]$^{\bullet}$ dimer was not detected in the UV-Vis-NIR absorption study. The reason behind can be related with the high intensity of the ν(C≡N) infrared band that makes this species to appear even when it might be presented in small amounts, which would explain that it is not recorded in the electronic absorption experiment.

Conclusions

Two molecular triads based on the diketopyrrolopyrrole unit centered between two quinoidal thienothiophene moieties terminally substituted with dicyano-methylene or phenoxyl groups have been synthetized. Spectroscopic studies at low temperatures have allowed to address the phenomenon of aggregation/dimerization in solution. The vibronic structures of the absorption spectra of the neutral molecules have been assigned to H-aggregates revealing the importance of the excitonic coupling in the dimers. Aggregation of these molecules has also been assessed in their charged anionic forms, for which dimers of two radical anions and also of one neutral molecule and one radical anion have been evidenced by the UV-Vis-NIR and the infrared spectra. Interestingly, this is one of the first cases where one system uses the same template for aggregation in the neutral state as well as in the charged state. In previous examples of similar molecules, either these aspects have been omitted or the neutral and anion species display different forms of supramolecular organization. In these dimeric forms, we further describe a variety of electron distributions which are responsible of a diversity of electronic absorption properties in the Vis-NIR and in the infrared parts of the spectrum. Species such as mixed valence open-shell radical anion dimers, dimeric singlet open-shell dianions in equilibrium with their single molecule charged species, radical anion and close-shell dianions, have identified all accommodated and embedded in such robust dimers.

These kind of studies are of interest given the new insights revealed here that certainly control the way of supramolecular organization of π-conjugated molecules in both neutral and charged states, which is of great importance to design a more precise engineering for constructing semiconducting organic materials.

Experimental Section

Synthesis and Chemical Characterization

^{1}H NMR data were recorded at 25 °C with a Bruker AC300 and A400 spectrometer with chemical shifts referenced to residual TMS. Matrix-assisted laser desorption/ionization time-of-flight (MALDI-TOF) mass spectra were obtained on a Bruker Microflex LRF20 instrument using dithranol as a matrix, and 4.8 eV under vacuum was established as the reference level. IR spectra were measured with a Nicolet Impact 400D spectrophotometer.

Synthesis of DPP-2

To a 25 mL round-bottom flask dibrominated **DPP-1** (0.118 mmol), boronic ester (0.596 mmol), two drops of Aliquat 336, and PPh_3 (0.094 mmol) were added under nitrogen atmosphere. Then, 6 mL of degassed toluene were added to the flask and the solution was degassed again. Afterwards, a degassed K_2CO_3 2 M solution (0.2 mL), and $Pd_2(dba)_3$ (0.012 mmol) solution in toluene (6 mL) were added to the reaction flask. The reaction was stirring overnight to 90 °C. After that, the crude was washed with water and extracted with CH_2Cl_2. The compound was purified by a silica gel column with $CHCl_3$ to give dark solid with 68% of yield. ^{1}H-NMR: (300 MHz, $CDCl_3$) δ (ppm): 9.37 (s, 2H), 7.48 (s, 4H), 7.41 (s, 2H), 5.43 (s, 2H), 4.11–4.08 (m, 4H), 1.99–1.97 (m, 2H), 1.50 (s, 36H), 1.43–1.25 (m, 16H), 0.94–0.85 (m, 12H). ^{13}C-NMR: ($CDCl_3$): δ (ppm) = 161.9, 154.9, 153.0, 144.7, 140.2, 138.9, 136.87, 136.85, 129.9, 128.0, 125.9, 123.5, 113.9, 108.3, 46.4, 39.4, 34.6, 30.4, 28.5, 23.8, 23.3, 14.2, 10.7. UV-vis (CH_2Cl_2): λ_{max} (nm) (log ε): 351 (4.67), 425 (4.36), 591 (4.89), 636 (4.97). FTIR (KBr) ν (cm^{-1}): 3633, 2957, 2926, 2870, 1660, 1578, 1466, 1427, 1398, 1240, 873–709. HR-MS (MALDI-TOF): 1043.4925 m/z (calcd for [M−H] 1043.4928).

Synthesis of DPP-TT-PhO

To a solution of bisphenol DDP-2 in CH_2Cl_2, PbO_2 (70 equ.) was added and the mixture was stirring for 30 min at r.t. Then, the PbO_2 excess was filtered off and the solvent was removed under reduced pressure. The compound was purified by silica gel column with $CHCl_3$ to give a dark solid with 95% of yield. UV-vis (CH_2Cl_2): λ_{max} (nm) (log ε): 573 (4.32), 725 (4.90), 783 (5.25). IR (KBr) ν (cm^{-1}): 2961, 2923, 2853, 1668, 1584, 1261, 1089, 1027, 875–703. HR-MS (MALDI-TOF): 1042.4789 m/z (calcd for $[M-H]^-$ 1042.4754).

Synthesis of DPP-TT-CN

In a round bottom flask, malononitrile (8.0 mg, 0.12 mmol) was added in a suspension of NaH (5.8 mg, 0.24 mmol) in 5 mL of anhydrous THF at 0 °C under an inert atmosphere. Then the reaction was heated at room temperature and stirred for 30 min. Simultaneously, in another round bottom flask, dibromo **DPP-1** (40 mg, 0.51 mmol), $Pd(PPh_3)_4$ catalyst (29 mg, 0.025 mmol) and 3 mL of THF were added. The reaction mixture was refluxed for 40 minutes and then the sodium malonate suspension was transferred to this flask and, lastly, the reaction was refluxed for a further 12 h. After that, it was cooled to 0 °C, exposed to air, and diluted in HCl 2 M (5 mL). Afterwards, the r.t. was reached and the reaction mixture was stirred for additional 8 h, the mixture was extracted with $CHCl_3$ and dried over Na_2SO_4. The purification was carried out by column chromatography on silica gel using CH_2Cl_2 as eluent afforded a green-red solid with 46% yield. ^{1}H-NMR: (300 MHz, CD_2Cl_2 + TFA-d) δ (ppm): 9.35 (d, J = 1.2 Hz, 2H), 9.24 (d, J = 0.9 Hz, 2H), 4.13–3.99 (m, 4H), 1.99–1.93 (m, 2H), 1.43–1.26 (m, 16H), 0.96–0.87 (m, 12H). ^{13}C-NMR: ($CDCl_3$ + TFA-d): δ (ppm): 176.8, 162.6, 161.9, 160.8, 160.3, 148.4, 137.0, 134.0, 132.7, 131.5, 120.1, 177.9, 108.7, 47.5, 39.5, 30.1, 28.3, 23.4, 23.2, 14.1, 10.3. UV-vis (CH_2Cl_2): λ_{max} (nm) (log ε): 400 (4.39), 420 (4.55), 697 (4.99), 795 (5.15). IR (KBr) ν (cm^{-1}): 259, 2924, 2853, 2208, 1688, 1503, 1466, 1263, 1125, 1090, 818–701. HR-MS (MALDI-TOF): 791.1866 m/z (calcd for $[M-H]^-$ 761.1865).

Measurements and Characterization

UV-Vis-NIR Temperature variable

Variable temperature UV-Vis-NIR electronic absorption spectra were recorded in a Varian Cary 5000 UV-Vis-NIR spectrophotometer with a wavelength range of 175–3300 nm using an Optistat DN cryostat from Oxford Instruments with a temperature stability of ±0.1 K. Spectra were obtained every 20 K on cooling waiting for 5 min until thermal equilibrium is achieved. Sample concentration was around 10^{-5} M. The temperature range was from room temperature (300 K) to 80 K in 2-methyl tetrahydrofurane purchased from Sigma-Aldrich/Merck (HPLC grade, 99%, spectroscopic degree).

Spectroelectrochemical Measurements

In situ IR and UV-Vis-NIR spectroelectrochemical studies were conducted on a VERTEX 70 FT-IR spectrometer and on a Varian Cary 5000 UV-Vis-NIR spectrophotometer, respectively. A C3 epsilon potentiostat from BASi was used for the electrolysis using a thin layer cell from a demountable omni cell from Specac. In this cell, a three-electrodes system was coupled to conduct in situ spectroelectrochemistry. A Pt gauze was used as the working electrode, a Pt wire was used as the counter electrode, and an Ag wire was used as the pseudo-reference electrode. The spectra were collected at constant potential electrolysis and the potentials were changed in intervals of 10 mV. The electrochemical medium used was 0.1 M tetrabutyl ammonium hexafluorophosphate, Bu_4NPF_6, in fresh distilled CH_2Cl_2, at room temperature with sample concentrations of 10^{-3} M.

Materials

All chemicals and solvents were purchased from Sigma Aldrich (Merck) and TCI and were used without further purification unless otherwise stated. **DPP** 1 was synthesized according to the literature.[29] Column chromatography was performed with SiO_2 (40–63 μm).

Electrochemistry

Cyclic voltammetry measurements were performed in 0.1 M Bu_4NPF_6 CH_2Cl_2 solutions as support electrolyte, a graphite working electrode, an Ag/Ag^+ reference electrode, and carbon counter electrode using a potentiostat/galvanostat μAutolab Type III. Ferrocene/ferrocenium redox couple (Fc/Fc^+) was used as an internal standard for all measurements.

Computational Details

Electronic structure calculations were carried out using Density Functional Theory (DFT) and its Time-Dependent extension (TD-DFT) as implemented in Gaussian16[41] at the CAM-B3LYP/6–31G(d,p) level of theory.[42–44] For calculations on dimers, GD3 dispersion corrections were added to account for van deer Waals interactions.[45]

Vibrationally resolved spectra of aggregates (Section II.2.2) were computed with an independent implementation of the excitonic model developed by Spano.[7] Vibronic spectra computed for monomers and dimers based on electronic structure calculations of the neutral and reduced species (Section II.3.2.) were calculated using the FCclasses3 code.[46] See SI for details.

Supporting Information

The Supporting Information is available free of charge. Synthesis and characterization data, experimental procedures and theoretical computational details. Additional references cited within the Supporting Information.[47–58]

Acknowledgements

The authors acknowledge financial support from MCIN/AEI of Spain (PID2021-127127NB-I00, PID2021-128569NB-I00, PID2020-117855RB-I00 and CEX2019-000919-M, funded by MCIN/AEI/10.13039/501100011033, "ERDF A way of making Europe", and "European Union NextGenerationEU/PRTR"), the Junta de Andalucía of Spain (PROYEXCEL-0328) and the Generalitat Valenciana (CIPROM/2021/059, MFA/2022/017 and MFA/2022/028). The MFA projects form part of the Advanced Materials program supported by MCIN with funding from European Union NextGenerationEU (PRTR–C17.I1) and by Generalitat Valenciana. Research Central Services (SCAI) of the University of Málaga and SuperComputing and BioInnovation Center (SCBI) are also acknowledged for the access to the facilities and computational resources, respectively. J.A. is indebted to the MCIN/AEI for his Ramón-y-Cajal (RyC-2017-23500) fellowship funded by MCIN/AEI/10.13039/501100011033 and by "ESF Investing in your future". D.A. acknowledges the Generalitat Valenciana and European Union-NextGenerationEU for postdoctoral contracts APOSTD/2021/025 and María Zambrano, respectively.

Conflict of Interests

The authors declare no competing financial interest.

Data Availability Statement

The data that support the findings of this study are available from the corresponding author upon reasonable request.

Keywords: aggregation · charged species · dimerization · diketopyrrolopyrrol · exciton coupling · quinoidal thiophenes · vibronic structure

[1] a) R. R. John, B. C. Thompson, T. A. Skotheim, *Handbook of Conducting Polymers*, 4th ed., CRC Press **2019**; b) G. Müllen, K. Wegner, *Electronic Materials: The Oligomeric Approach*, 1st ed., Wiley **1998**■■Please provide the publisher location for Ref. 1.■■.
[2] A. D. Scaccabarozzi, A. Basu, F. Aniés, J. Liu, O. Zapata-Arteaga, R. Warren, Y. Firdaus, M. I. Nugraha, Y. Lin, M. Campoy-Quiles, N. Koch, C. Müller, L. Tsetseris, M. Heeney, T. D. Anthopoulos, *Chem. Rev.* **2022**, *122*, 4420–4492.
[3] a) L. Wang, M. H. Yoon, A. Facchetti, T. Marks, *Adv. Mater.* **2007**, *19*, 3252–3256; b) H. Yan, Z. H. Chen, Y. Zheng, C. Newman, J. R. Quinn, F. Dötz, M. Kastler, A. Facchetti, *Nature* **2009**, *457*, 579–686.
[4] a) D. D. Graf, J. P. Campbell, L. L. Miller, *J. Am. Chem. Soc.* **1997**, *118*, 5480–5481; b) D. D. Graf, R. G. Duan, J. P. Campbell, L. L. Miller, K. R. Mann, *J. Am. Chem. Soc.* **1997**, *119*, 5888–5899.
[5] a) F. Würthner, T. E. Kaiser, C. R. Saha-Möller, *Angew. Chem. Int. Ed.* **2011**, *50*, 3376–3410; b) S. Ma, S. Du, G. Pan, S. Dai, B. Xu, W. Tian, *Aggregate* **2021**, e96■■Please provide the volume number for Ref. 5b.■■.
[6] a) M. Kasha, *Radiat. Res.* **1963**, *20*, 55–70; b) M. Kasha, H. R. Rawls, M. A. Bayoumi, *Pure Appl. Chem.* **1965**, *11*, 371–392; c) A. Diaz-Andres, J. Marín-Beloqui, J. Wang, J. Liu, J. Casado, D. Casanova, *Chem. Sci.* **2023**, *14*, 6420–6429.
[7] F. C. Spano, *Acc. Chem. Res.* **2010**, *43*, 429–439.
[8] N. J. Hestand, F. C. Spano, *Chem. Rev.* **2018**, *118*, 7069–7163.
[9] F. C. Spano, *J. Am. Chem. Soc.* **2009**, *131*, 4267–4278.
[10] M. Más-Montoya, R. A. J. Janssen, *Adv. Funct. Mater.* **2017**, *27*, 1605779.
[11] J. Casado, R. Ponce Ortiz, J. T. Navarrete, *Chem. Soc. Rev.* **2012**, *41*, 5672–5686.
[12] a) T. M. Pappenfus, R. J. Chesterfield, C. D. Frisbie, K. R. Mann, J. Casado, J. D. Raff, L. L. Miller, *J. Am. Chem. Soc.* **2002**, *124*, 4184–4185; b) R. J. Chesterfield, C. R. Newman, T. M. Pappenfus, P. C. Ewbank, M. H. Haukaas, K. R. Mann, L. L. Miller, C. D. Frisbie, *Adv. Mater.* **2003**, *15*, 1278–1282.
[13] T. Takahashi, K. Matsuoka, K. Takimiya, T. Otsubo, Y. Aso, *J. Am. Chem. Soc.* **2005**, *127*, 8928–8929.
[14] a) J. C. Ribierre, S. Watanabe, M. Matsumoto, T. Muto, A. Nakao, T. Aoyama, *Adv. Mater.* **2010**, *22*, 4044–4048; b) J. C. Ribierre, T. Fujihara, S. Watanabe, M. Matsumoto, T. Muto, A. Nakao, T. Aoyama, *Adv. Mater.* **2010**, *22*, 1722–1726.
[15] C. R. Newman, C. D. Frisbie, D. A. Da Silva, J.-L. Brédas, P. C. Ewbank, K. R. Mann, *Chem. Mater.* **2004**, *16*, 4436–4451.
[16] V. Coropceanu, J. Cornil, D. A. da Silva, Y. Olivier, R. Silbey, J.-L. Brédas, *Chem. Rev.* **2007**, *107*, 926–952.
[17] S. Handa, E. Miyazaki, K. Takimiya, Y. Kunugi, *J. Am. Chem. Soc.* **2007**, *129*, 11684–11685.
[18] a) K. Yamamoto, Y. Ie, M. Nitani, N. Tohnai, F. Kakiuchi, K. Zhang, W. Pisula, K. Asadi, P. W. M. Blom, Y. Aso, *J. Mater. Chem. C* **2018**, *6*, 7493; b) K. Yamamoto, S. Jinnai, T. Takehara, T. Suzuki, Y. Ie, *Org. Lett.* **2020**, *22*, 547.
[19] W. Wang, L. Ge, G. Xue, F. Miao, P. Chen, H. Chen, Y. Lin, Y. Ni, J. Xiong, Y. Hu, J. Wu, Y. Zheng, *Chem. Commun.* **2020**, *56*, 1405–1408.
[20] a) E. V. Canesi, D. Fazzi, L. Colella, C. Bertarelli, C. Castiglioni, *J. Am. Chem. Soc.* **2012**, *134*, 19070–19083; b) F. Liu, G. L. Espejo, S. Qiu, M. Moreno Oliva, J. Pina, J. S. Seixas de Melo, J. Casado, X. Zhu, *J. Am. Chem. Soc.* **2015**, *137*, 10357–10366.
[21] M. G. Hill, J. F. Penneau, B. Zinger, K. R. Mann, L. L. Miller, *Chem. Mater.* **1992**, *4*, 1106–1113.
[22] a) R. Mann, L. L. Miller, J. Francois Penneau, *J. Am. Chem. Soc.* **1992**, *114*, 2728–2730; b) D. D. Graf, R. G. Duan, J. P. Campbell, L. L. Miller, K. R. Mann, *J. Am. Chem. Soc.* **1997**, *119*, 5888–5899.
[23] a) P. Bauerle, U. Segebacher, A. Maier, M. Mehring, *J. Am. Chem. Soc.* **1993**, *115*, 10217–10223; b) J. van Haare, E. E. Havinga, J. L. J. van Dongen, R. A. J. Janssen, J. Cornil, J. L. Brédas, *Chem. Eur. J.* **1998**, *4*, 1509–1522.
[24] R. Rausch, M. I. S. Röhr, D. Schmidt, I. Krummenacher, H. Braunschweig, F. Wurthner, *Chem. Sci.* **2021**, *12*, 793–802.
[25] C. Wang, Y. Zang, Y. Qin, Q. Zhang, Y. Sun, C. Di, W. Xu, D. Zhu, *Chem. Eur. J.* **2014**, *20*, 13755–13761.
[26] a) S. Ray, S. Sharma, U. Salzner, S. Patil, *J. Phys. Chem. C* **2017**, *121*, 16088–16097; b) S. Ghosh, S. Cherumukkil, C. H. Suresh, A. Ajayaghosh, *Adv. Mater.* **2017**, *29*, 1703783.
[27] a) Y. Zang, E. Gann, C. R. McNeill, X. Xhu, C. Di, D. Zhu, *J. Am. Chem. Soc.* **2014**, *136*, 16176–16184; b) C. Wang, Y. Qin, Y. Sun, Y. S. Guan, W. Yu, D. Zhu, *Appl. Mater. Interferences* **2015**, *7*, 15978–15978.
[28] Y. Qiao, Y. Guo, C. Yu, F. Zhang, W. Yu, Y. Lui, D. Zhu, *J. Am. Chem. Soc.* **2012**, *134*, 4084–4087.
[29] R. Rausch, M. I. S. Röhr, D. Schmidt, I. Krummenacher, H. Braunschweig, F. Würthner, *Chem. Sci.* **2021**, *12*, 793–802.
[30] F. J. A. Ferrer, F. Santoro, *Phys. Chem. Chem. Phys.* **2012**, *14*, 13549–13563.
[31] J. Cerezo, F. Santoro, *J. Comput. Chem.* **2023**, *44*, 626–643.
[32] P. E. Hartnett, S. M. Dyar, E. A. Margulies, L. E. Shoer, A. W. Cook, S. W. Eaton, T. J Marks, M. R. Wasielewski, *Chem. Sci.* **2015**, *6*, 402–411.
[33] J. Casado, L. L. Miller, K. R. Mann, T. M. Pappenfus, H. Higuchi, E. Orti, B. Milian, R. Pou-Amerigo, V. Hernandez, J. T. L. Navarrete, *J. Am. Chem. Soc.* **2002**, *124*, 12380–12388.

[34] T. M. Pappenfus, J. D. Raff, E. J. Hukkanen, J. R. Burney, J. Casado, S. M. Drew, L. L. Miller, K. R. Mann, *J. Org. Chem.* **2002**, *67*, 6015–6024.
[35] J. Casado, M. Z. Zgierski, P. C. Ewbank, M. W. Burand, D. E. Janzen, K. R. Mann, T. M. Pappenfus, A. Berlin, E. Perez-Inestrosa, R. P. Ortiz, J. T. L. Navarrete, *J. Am. Chem. Soc.* **2006**, *128*, 10134–10144.
[36] S. Medina Rivero, L. Rin, M. E. Sandoval-Salinas, S. J. Grabowski, D. Casanova, X. Zhu, J. Casado, *Chem. Eur. J.* **2018**, *24*, 13523–13534.
[37] S. Medina Rivero, W. Liu, D. Casanova, X. Zhu, J. Casado, *Angew. Chem. Int. Ed.* **2019**, *58*, 11291–11295.
[38] Y. Furukawa, *J. Phys. Chem.* **1996**, *100*, 15644–15653.
[39] A. Sakamoto, Y. Furukawa, M. Tasumi, *J. Phys. Chem.* **1992**, *96*, 3870–3874.
[40] Y. Liu, D. Aranda, F. Santoro, *Phys. Chem. Chem. Phys.* **2021**, *23*, 16551–16563.
[41] M. J. Frisch, G. W. Trucks, H. B. Schlegel, G. E. Scuseria, M. A. Robb, J. R. Cheeseman et al., *Gaussian 16, Revision A.03*. Gaussian, Inc., Wallingford, CT **2016**.
[42] T. Yanai, D. P. Tew, N. C. Handy, *Chem. Phys. Lett.* **2004**, *393*, 51–57.
[43] W. J. Hehre, R. Ditchfield, J. A. Pople, *J. Chem. Phys.* **1972**, *56*, 2257.
[44] P. C. Hariharan, J. A. Pople, *Theor. Chem. Acc.* **1973**, *28*, 213–22.
[45] S. Grimme, J. Antony, S. Ehrlich, H. Krieg, *J. Chem. Phys.* **2010**, *132*, 154104.
[46] J. Cerezo, F. Santoro, *J. Comput. Chem.* **2023**, *44*(4), 626–643.
[47] M. J. Frisch, G. W. Trucks, H. B. Schlegel, G. E. Scuseria, M. A. Robb, J. R. Cheeseman et al., *Gaussian 16, Revision A.03*. Gaussian, Inc., Wallingford, CT **2016**.
[48] T. Yanai, D. P. Tew, N. C. Handy, *Chem. Phys. Lett.* **2004**, *393*, 51.
[49] W. J. Hehre, R. Ditchfield, J. A. Pople, *J. Chem. Phys.* **1972**, *56*, 2257.
[50] P. C. Hariharan, J. A. Pople, *Theor. Chem. Acc.* **1973**, *28*, 213.
[51] F. J. Avila, F. Santoro, *Phys. Chem. Chem. Phys.* **2012**, *14*, 13549.
[52] J. Cerezo, F. Santoro, *J. Chem. Theory Comput.* **2016**, *12*(10), 4970.
[53] J. Cerezo, D. Aranda, F. J. Avila, G. Prampolini, F. Santoro, *J. Chem. Theory Comput.* **2020**, *16*(2), 1215.
[54] N. J. Hestand, F. Spano, *Chem. Rev.* **2018**, *118*(15), 7069.
[55] M. F. Iozzi, B. Mennucci, J. Tomasi, R. Cammi, *J. Chem. Phys.* **2004**, *120*, 7029.
[56] P. E. Hartneet, E. A. Margulies, C. M. Mauck, S. A. Miller, Y. Wu, Y.-L. Wu, T. J. Marks, M. R. Wasielewski, *J. Phys. Chem. B* **2016**, *120*(7), 1357.
[57] E. F. Pettersen, T. D. Goddard, C. C. Huang, E. C. Meng, G. S. Couch, T. I. Croll, et al., *Protein Sci.* **2021**, *30*, 70.
[58] A. J. Schaefer, V. M. Ingman, S. E. Wheeler, *SEQCROW: J. Comp. Chem.* **2021**, *42*, 1750.

Manuscript received: May 29, 2024
Accepted manuscript online: July 19, 2024
Version of record online: ■■, ■■

RESEARCH ARTICLE

Diketopyrrolopyrrol quinoidal oligomers aggregate in a very similar way in the neutral state and in the dimer dianion states due to an uniform distribution of the electron charge excess between the two molecules in the dimer dianion.

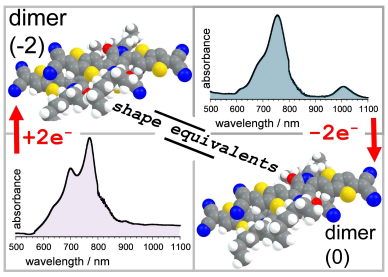

S. Moles Quintero, M. João Álvaro-Martins, D. Aranda, Y. Zheng, J. Aragó, E. Ortí, Á. Sastre Santos*, J. Casado**

1 – 14

Neutral and Anion Species of Quinoidal Thienothiophene Diketopyrrolopyrroles Display a Common Aggregation Mode

SPACE RESERVED FOR IMAGE AND LINK

Share your work on social media! *Chemistry - A European Journal* has added Twitter as a means to promote your article. Twitter is an online microblogging service that enables its users to send and read short messages and media, known as tweets. Please check the pre-written tweet in the galley proofs for accuracy. If you, your team, or institution have a Twitter account, please include its handle @username. Please use hashtags only for the most important keywords, such as #catalysis, #nanoparticles, or #proteindesign. The ToC picture and a link to your article will be added automatically, so the **tweet text must not exceed 250 characters**. This tweet will be posted on the journal's Twitter account (follow us @ChemEurJ) upon publication of your article in its final form. We recommend you to re-tweet it to alert more researchers about your publication, or to point it out to your institution's social media team.

ORCID (Open Researcher and Contributor ID)

Please check that the ORCID identifiers listed below are correct. We encourage all authors to provide an ORCID identifier for each coauthor. ORCID is a registry that provides researchers with a unique digital identifier. Some funding agencies recommend or even require the inclusion of ORCID IDs in all published articles, and authors should consult their funding agency guidelines for details. Registration is easy and free; for further information, see http://orcid.org/.

Maria João Álvaro-Martins
Enrique Ortí
Juan Aragó
Juan Casado http://orcid.org/0000-0003-0373-1303
Sergio Moles Quintero
Yonghao Zheng
Ángela Sastre Santos
Daniel Aranda